nature portfolio

https://doi.org/10.1038/s41586-022-05612-1

Supplementary information

Vertical full-colour micro-LEDs via 2D materials-based layer transfer

In the format provided by the authors and unedited

Supplementary Note 1. Comparison of remote epitaxy and van der Waals epitaxy

As both remote epitaxy and van der Waals epitaxy allow for the exfoliation of epilayers at the 2D interface, both techniques can be used for the fabrication of vertically stacked μLEDs. We employed van der Waals epitaxy of InGaN-based blue LEDs for reasons of technical maturity, as the technique was reported previously[1]. For III-V red LEDs, it would be difficult to grow the structure by van der Waals epitaxy, because GaAs (100) has zinc-blende (cubic) lattices unlike 2D materials (graphene and hBN) that exhibit hexagonal in-plane lattices. In other words, the hexagonal 2D layers cannot work as a seed layer, and remote interaction is necessary for the growth of (100) oriented thin films. We therefore employed remote epitaxy of red LEDs, which has been reported previously[2].

The crystalline quality of LEDs obtained via van der Waals epitaxy does resemble that of the hBN layers, as there is orientational guidance from the hBN. Depending on the crystalline quality of hBN, varying degrees of misorientation spread are observed in the III-nitrides. Beyond a certain crystallinity limit of hBN, the III-nitrides grown could be even amorphous. This effect has been demonstrated in a previous article[3], where III-nitrides were grown on hBN on c-plane sapphire and dielectric patterns. Therefore, it is crucial to grow hBN layers with a good crystal quality. In our current work, we optimized hBN growth conditions, which resulted in our blue LEDs showing EQEs as high as control samples grown on a bare sapphire substrate as shown in Extended Data Figs. 3g-h.

Broader EL spectra and larger rms roughness of blue and green LEDs grown on hBN/sapphire wafers (Figs. 2n-o, Extended Data Figs. 2k-l) are caused by the roughness of AlGaN layer. Nucleation of AlGaN on hBN occurs via lateral growth and coalescence of islands with different sizes, which leads to the formation of rough AlGaN surface (see Supplementary Figs. 3c-d). However, these problems may be addressed via the remote epitaxy of InGaN-based LEDs, as shown in Extended Data Fig. 9.

Supplementary Note 2. Throughput of 2DLT process

High speed and yield of exfoliation process are key advantages of 2D materials-based layer transfer (2DLT). Compared with other lift-off techniques such as chemical lift-off (also known as epitaxial lift-off (ELO)), laser lift-off (LLO), and controlled mechanical spalling, 2DLT is capable of the fastest layer release, because the propagation of crack through the 2D layer occurs in timescales of less than 1 second, as illustrated in our Supplementary Video 1. Controlled mechanical spalling also achieves similar release speeds as it shares the same release mechanism[4], but is limited by the inability to control exactly the thickness of the released film. A reported rate of LLO process, for 6'' wafers using 248 nm excimer laser at 50 Hz pulse frequency[5], is 45 seconds per wafer, which includes the time needed to scan the laser over the entire area of the wafer. The interface side of the film exfoliated by the LLO process is also roughened by laser ablation, often necessitating post-processing for device fabrication. ELO requires the longest time for layer release, ranging from several hours to a day per wafer[6], due to the slow rates of lateral diffusion of HF during wet chemical etching of sacrificial Al(Ga)As layer. Therefore, among lift-off techniques, 2DLT offers the highest throughput for producing ultrathin, freestanding LED membranes.

Supplementary Note 3. Discussion on luminance and EQEs on RGB μLEDs obtained via 2DLT

Extended Data Figs. 3a-d show the luminance measured for red, green, blue, and reference μLEDs of varying size, ranging from 4×4 μm^2 to 15×16 μm^2, that correspond to the sizes demonstrated in Fig. 4e. The luminance of our red μLEDs are within the range of 10^4-10^5 cd/m^2, while those of green and blue μLEDs are 10^6-10^7 cd/m^2, both of which meet ~10^5 cd/m^2 luminance required for augmented and mixed reality display applications[7]. The luminance of reference blue μLEDs are also in the similar range but at higher current densities, which may be due to lower power efficiency. Our results show a lack of size dependence, both for devices obtained via 2DLT and those grown via direct heteroepitaxy.

Extended Data Figs. 3e-h show that the EQEs of our red, green, blue, and reference μLEDs are roughly 0.03 %, 0.10 %, 0.20 %, and 0.05 %, respectively. These low efficiencies can be mainly attributed to the fact that we have adopted the simplest LED structures that yield light emission, as the main focus of this study was to prepare ultrathin, single-crystalline, releasable, and stackable layers of RGB LEDs using 2D materials. The low EQEs of blue LEDs with identical structure grown directly on sapphire substrate are also indicative of this. The lack of size dependence for EQEs in all our devices may also be due to the inherent low efficiencies overshadowing the effects of non-radiative recombination on sidewalls. Our strategy of vertically stacking μLEDs still offers a way to potentially reduce these effects, as the μLEDs can be 3x larger than those in laterally assembled μLEDs of the same PPI. Enhancing the efficiencies may require better optimization of QW/QB layers for red LEDs, electron blocking layers and p-GaN contact layers with a doping gradient for blue and green LEDs, out-coupling structures such as lens or roughened surface, distributed Bragg reflectors, and high-transparency conductive oxides such as AZO or ITO.

Supplementary Note 4. Reusability of substrate following 2DLT

The high cost of wafer reuse process for lift-off techniques such as ELO, LLO, and controlled mechanical spalling is due to the need for chemical mechanical polishing (CMP) to reconstruct epi-ready surface, as the wafer surface becomes too rough for high-quality epitaxy after lift-off [4,8,9]. CMP is known as an expensive process with high costs of equipment, consumables, maintenance and replacement. Nonetheless, National Renewable Energy Laboratory has reported in 2018 that at sufficiently low polishing cost and large number of substrate re-uses, CMP may still significantly reduce manufacturing costs of III-V solar cells[10].

Compared to above-mentioned techniques, substrate reuse is much simpler and cheaper for 2DLT. In Figs. 2p-s and Extended Data Fig. 4, we have shown that the hBN/sapphire substrate can be reused following the exfoliation of LED layer by sputtering a Ni stressor layer, peeling off the hBN layer using tape, and wet etching to remove any metal residue. These steps, which cost less time and money compared to CMP, return the sapphire substrate to epi-ready state with rms roughness of 0.375 nm. Similarly simple and low-cost reuse of GaAs substrates following remote epitaxy of GaAs membranes has also been reported recently[11], whereby graphene layer is removed by oxygen plasma.

These processes are cheaper, more scalable, and less time-consuming than CMP, which suggests that wafer reusability can be a key advantage of 2DLT over other lift-off techniques. Moreover, while CMP reduces the substrate thickness after each polish, which eventually limits the total number of wafer re-uses possible, 2DLT re-use process doesn't. Lastly, unlike existing lift-off techniques, 2DLT has the potential to be used for epitaxy on significantly more expensive GaN wafers to yield high-performance devices, in which case the wafer re-use becomes more important.

Supplementary Note 5. Calculation of RGB color purities

The color purity for the µLED was calculated by the following equation:

$$\text{Color purity} = \frac{\sqrt{(x - x_{ee})^2 + (y - y_{ee})^2}}{\sqrt{(x_d - x_{ee})^2 + (y_d - y_{ee})^2}}$$

where (x, y) are chromaticity coordinates of the fabricated µLEDs, (x_{ee}, y_{ee}) are coordinates for the equal-energy illuminant, which is (0.333, 0.333), and (x_d, y_d) are coordinates for dominant wavelength coordinates, which is the point at which a straight line passes through the intersection of (x, y) and (x_{ee}, y_{ee}) in the chromaticity diagram. The RGB color coordinates of (0.676, 0.285), (0.307, 0.656), and (0.145, 0.066), yield RGB color purities of 88.3 %, 90.5 %, and 94.1 %, respectively.

Supplementary Note 6. Remote epitaxy of InGaN-based LEDs on GaN wafers

Extended Data Fig. 9a shows the epitaxial structure of InGaN-based blue LED grown by remote epitaxy. The results of AFM and ECCI analyses in Extended Data Figs. 9b-c reveal a significantly smoother surface morphology (RMS roughness: 0.792 nm) as well as lower dislocation density for GaN epilayers obtained via remote epitaxy over those obtained via van der Waals epitaxy, indicating superior material quality of the former. Moreover, the EQE and luminance of the fabricated blue µLEDs are ~0.3 % and ~10^7 Cd/m^2, respectively, which is roughly 1.5 times and 1 order of magnitude higher than those of blue µLEDs grown on hBN/sapphire (Extended Data Figs. 3g and 3c). These results indicate that remote epitaxy of III-nitride LEDs may improve both the material quality and device performance of blue and green LEDs.

References

1. Ayari, T. *et al.* Wafer-scale controlled exfoliation of metal organic vapor phase epitaxy grown InGaN/GaN multi quantum well structures using low-tack two-dimensional layered h-BN. *Applied Physics Letters* **108**, 171106 (2016).
2. Kim, Y. *et al.* Remote epitaxy through graphene enables two-dimensional material-based layer transfer. *Nature* **544**, 340-343 (2017).
3. Sundaram, S. *et al.* MOVPE of GaN-based mixed dimensional heterostructures on wafer-scale layered 2D hexagonal boron nitride—A key enabler of III-nitride flexible optoelectronics. *APL Materials* **9**, 061101 (2021).
4. Chen, J. & Packard, C. E. Controlled spalling-based mechanical substrate exfoliation for III-V solar cells: A review. *Solar Energy Materials and Solar Cells* **225**, 111018 (2021).
5. Delmdahl, R. *et al.* Line beam processing for laser lift-off of GaN from sapphire. *physica status solidi (a)* **209**, 2653-2658 (2012).
6. Kim, Y. *et al.* Internal stress-assisted epitaxial lift-off process for flexible thin film (In)GaAs solar cells on metal foil. *Applied Physics Letters* **111**, 233509 (2017).
7. Lee, V. W., Twu, N. & Kymissis, I. Micro-LED technologies and applications. *Information Display* **32**, 16-23 (2016).
8. Zhang, B., Luo, C. & Li, Y.-F. Damage-free transfer of GaN-based light-emitting devices and reuse of sapphire substrate. *ECS Journal of Solid State Science and Technology* **9**, 065019 (2020).
9. Bauhuis, G. J. *et al.* Wafer reuse for repeated growth of III–V solar cells. *Progress in Photovoltaics: Research and Applications* **18**, 155-159 (2010).
10. Horowitz, K. A., Remo, T. W., Smith, B. & Ptak, A. J. A techno-economic analysis and cost reduction roadmap for III-V solar cells. Medium: ED; Size: 35 p. (United States, 2018).
11. Kim, H. *et al.* Multiplication of freestanding semiconductor membranes from a single wafer by advanced remote epitaxy. *arXiv preprint arXiv:2204.08002* (2022).

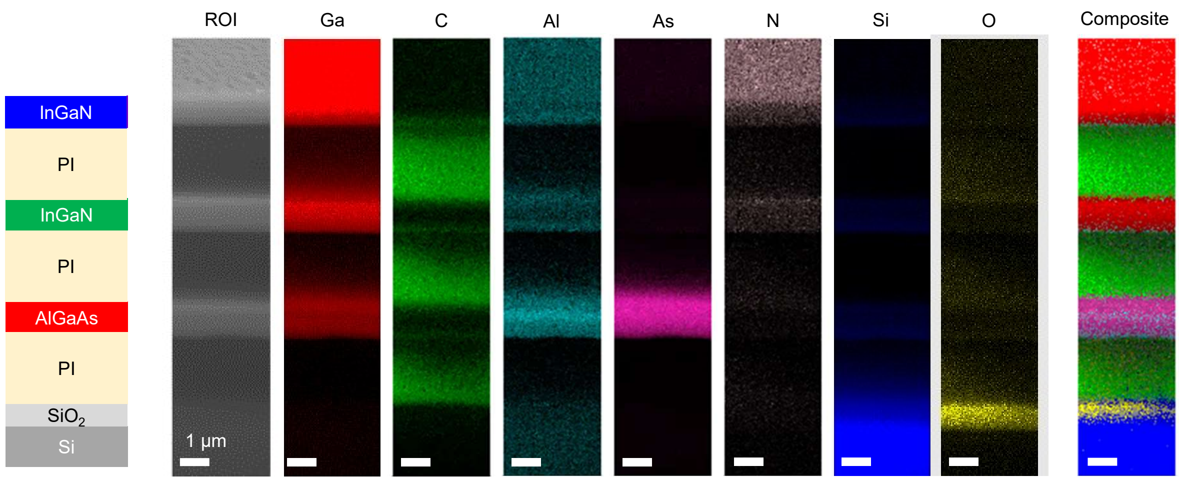

Supplementary Figure 1 | SEM-EDX elemental maps illustrating layer-by-layer material composition of vertically-stacked RGB LED films.

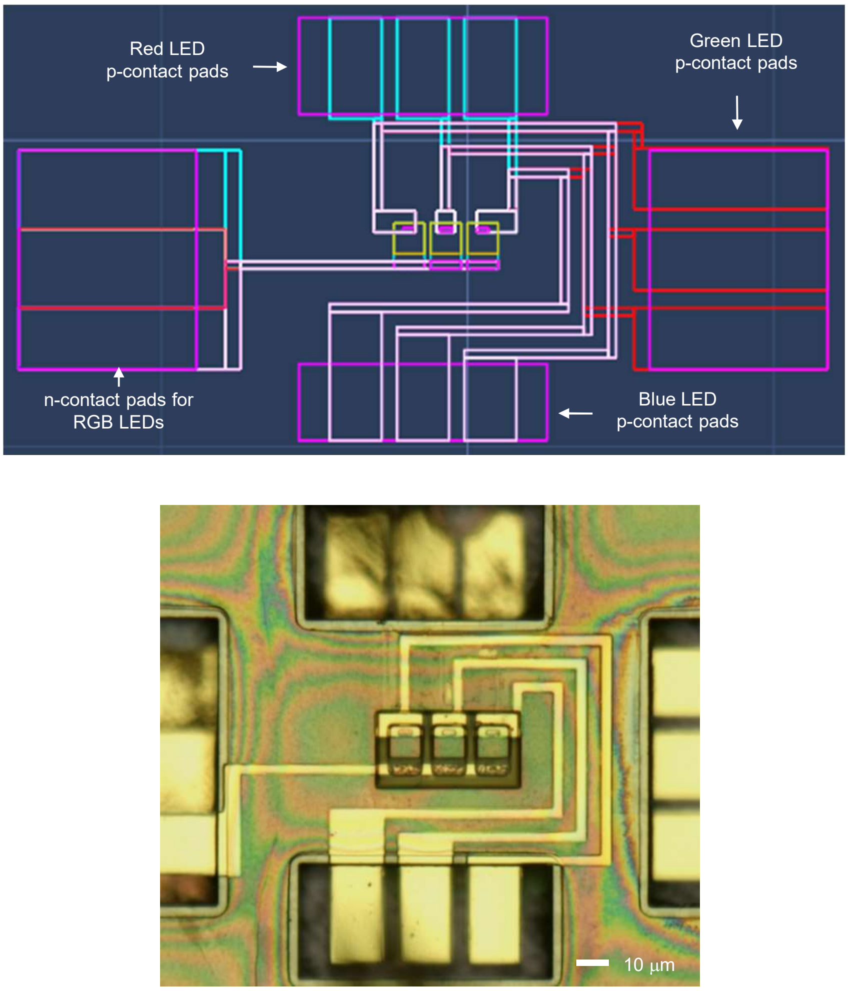

Supplementary Figure 2 | CAD design image and optical microscope image of three parallel vertical μLED pixels illustrating the arrangement of metal contacts.

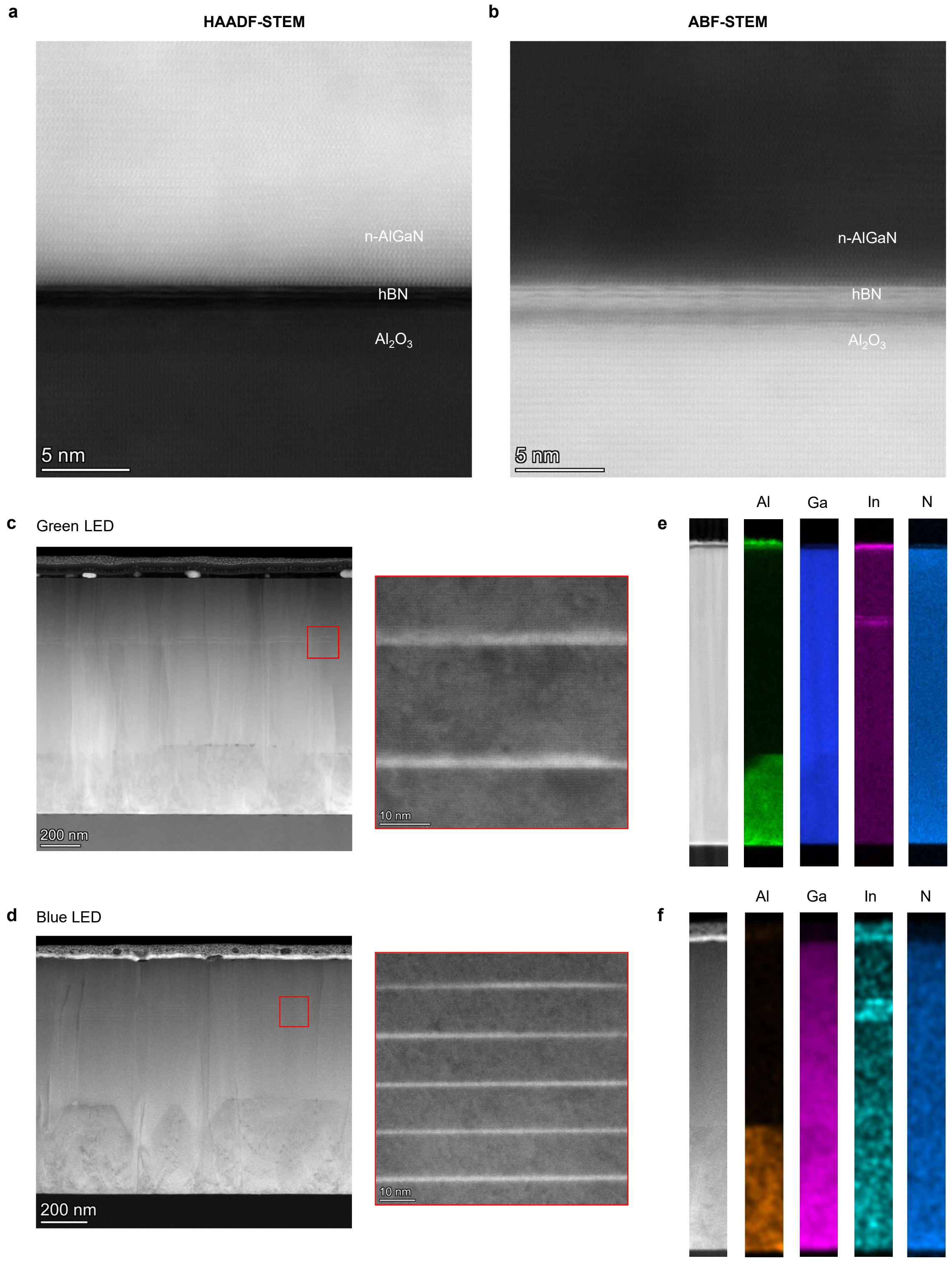

Supplementary Figure 3 | STEM and EDX analysis of InGaN-based blue and green LEDs obtained via 2DLT. a-b, High angle annular dark field (HAADF)-STEM (a) and annular bright field (ABF)-STEM (b) images of the LED-hBN-substrate interface region illustrating formation of smooth hBN layer. **c-d**, STEM images highlighting the MQWs of green (c) and blue (d) LEDs. **e-f**, EDX elemental maps for green (e) and blue (f) LEDs.

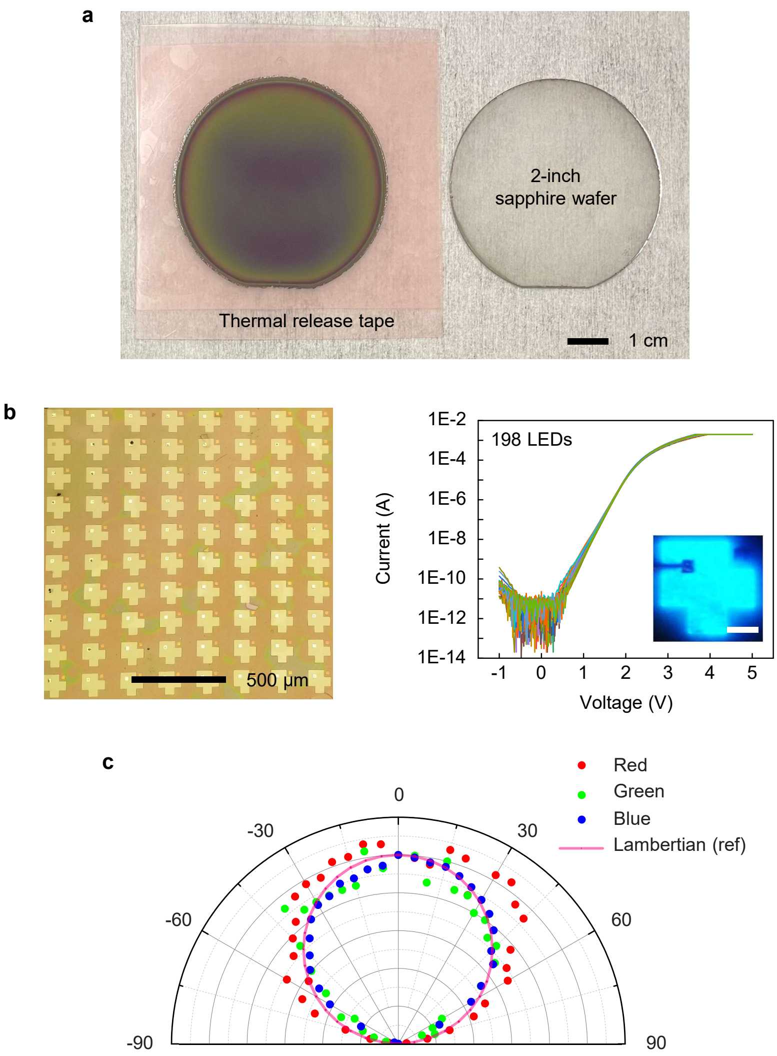

Supplementary Figure 4 | Evaluation of process yields and radiation patterns of RGB μLEDs obtained via 2DLT. a, Photograph of 2-inch wafer-scale blue LED film exfoliated from hBN-coated sapphire substrate following deposition of Ni stressor layer, indicating no sign of physical damage. **b**, Optical microscope image (left) and representative I-V curves (right) of blue μLEDs fabricated after transfer onto Si wafer. The I-V characteristics of 198 functional μLEDs (out of 200 transferred) show high uniformity. Inset, EL image of a blue μLED device. Scale bar, 50 μm. **c**, Radiation patterns of vertically stacked red, green, and blue μLEDs measured every 5º from -90º to +90º. compared with Lambertian emission profile (pink line, ref).

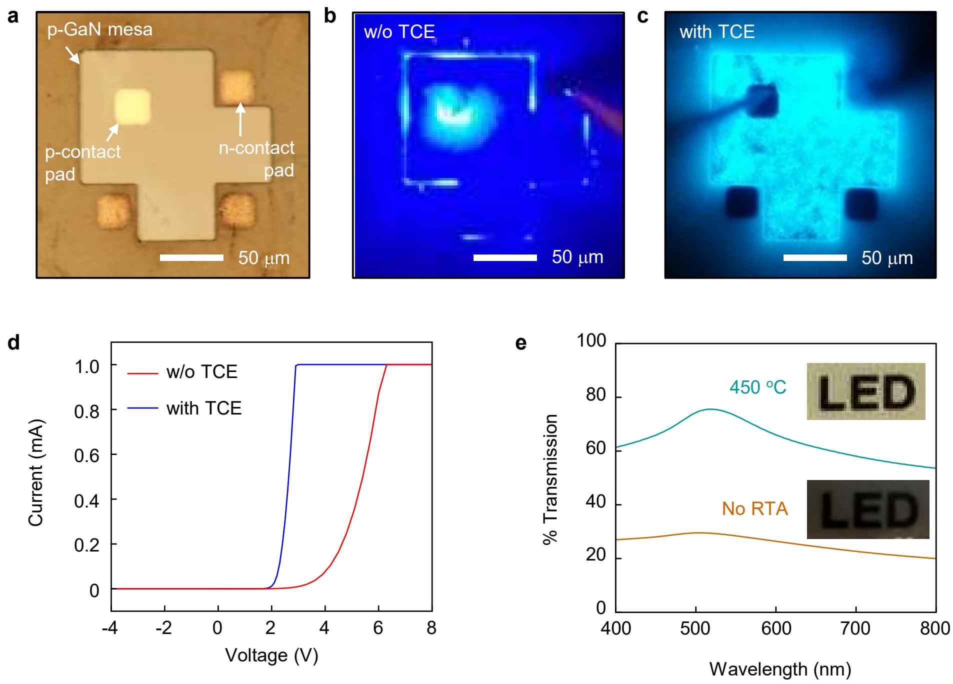

Supplementary Figure 5 | Importance of Ni/Au transparent conductive electrode for current spreading on p-GaN layer. a, Optical microscope image of a representative InGaN-based blue LED device with p-GaN layer on top. **b-c**, EL microscope images of blue LEDs without (b) and with (c) Ni/Au transparent conductive electrode (TCE) on p-GaN mesa. **d**, I-V curves obtained from blue LEDs with (blue line) and without (red line) TCE. **e**, Optical transmission spectra of Ni/Au TCE before and after RTA at 450 °C. Insets, Photographs of printed letters 'LED' covered on top by glass slides coated with Ni/Au TCE before (bottom) and after (top) RTA.

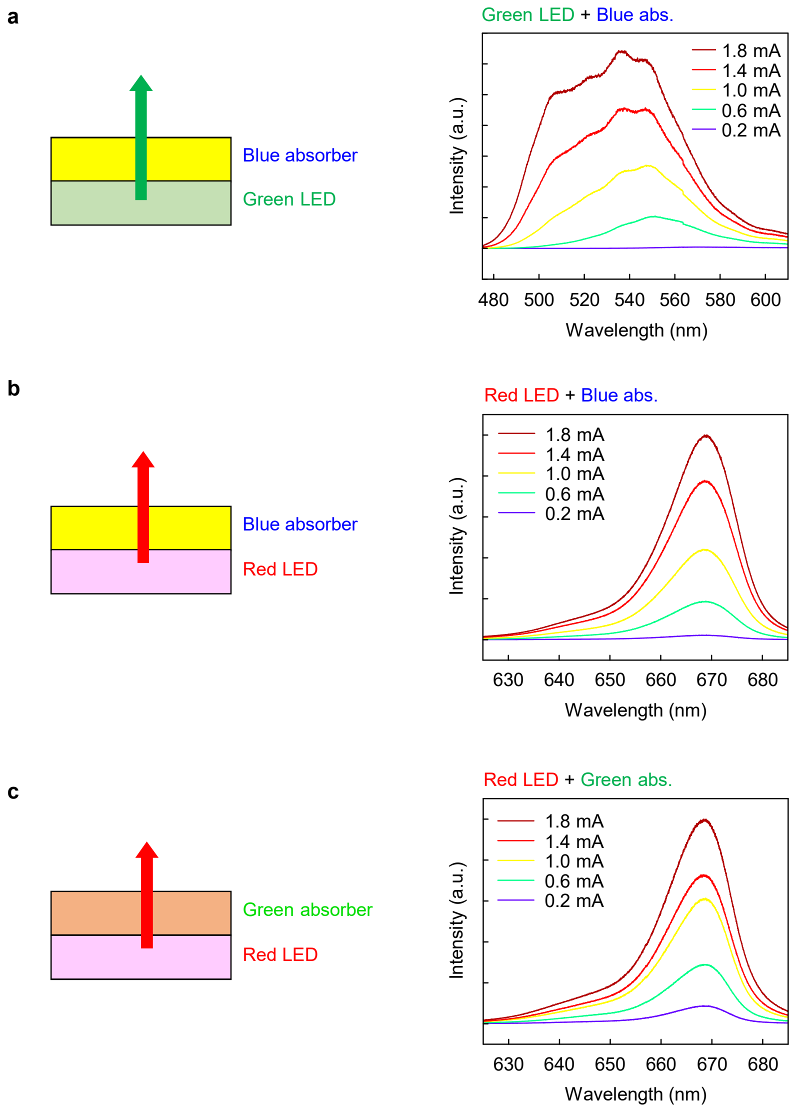

Supplementary Figure 6 | High transmission of upward emissions by blue and green absorbers. a-c, Schematic illustrations (left) and normalized EL spectra (right) collected under varying levels of injection current for a green LED coated with blue absorber layer (a) and red LEDs coated with blue (b) or green (c) absorber layers.

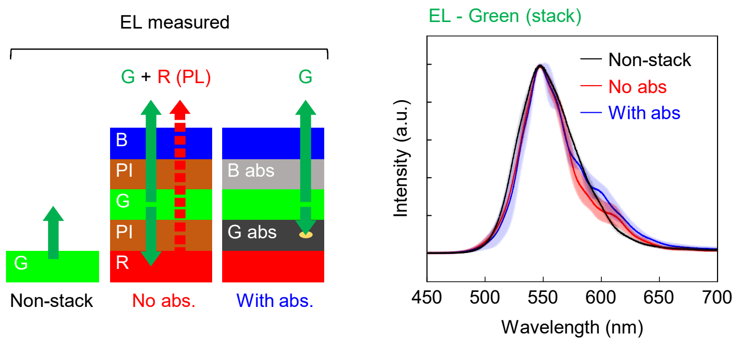

Supplementary Figure 7 | Prevention of photoluminescence in vertically stacked LEDs via absorber. Schematic illustrations (left) and recorded EL spectra (right) for transferred, non-stacked green μLED (Non-stack; black), green μLED integrated in a vertical stack using PI adhesive layer (No abs; red), and green μLED integrated in a vertical stack with green absorber (With abs; blue). Error bars represent the SD for at least three measurements.

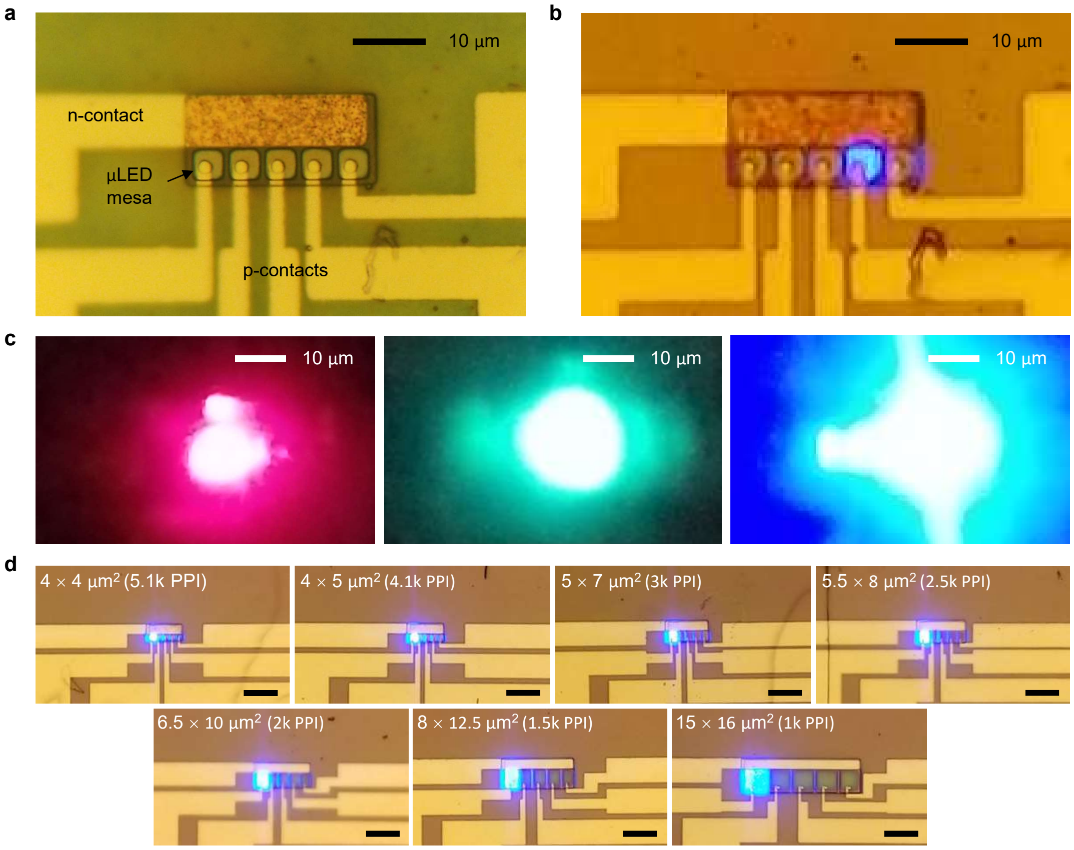

Supplementary Figure 8 | Electroluminescence microscopy images of RGB μLEDs of varying dimensions. a-b, Optical (a) and EL (b) microscopy image of 4 × 4 μm^2-sized blue μLEDs. **c**, EL images of RGB μLEDs in dark. **d**, EL microscopy images of blue μLEDs with varying size. Scale bar, 25 μm.

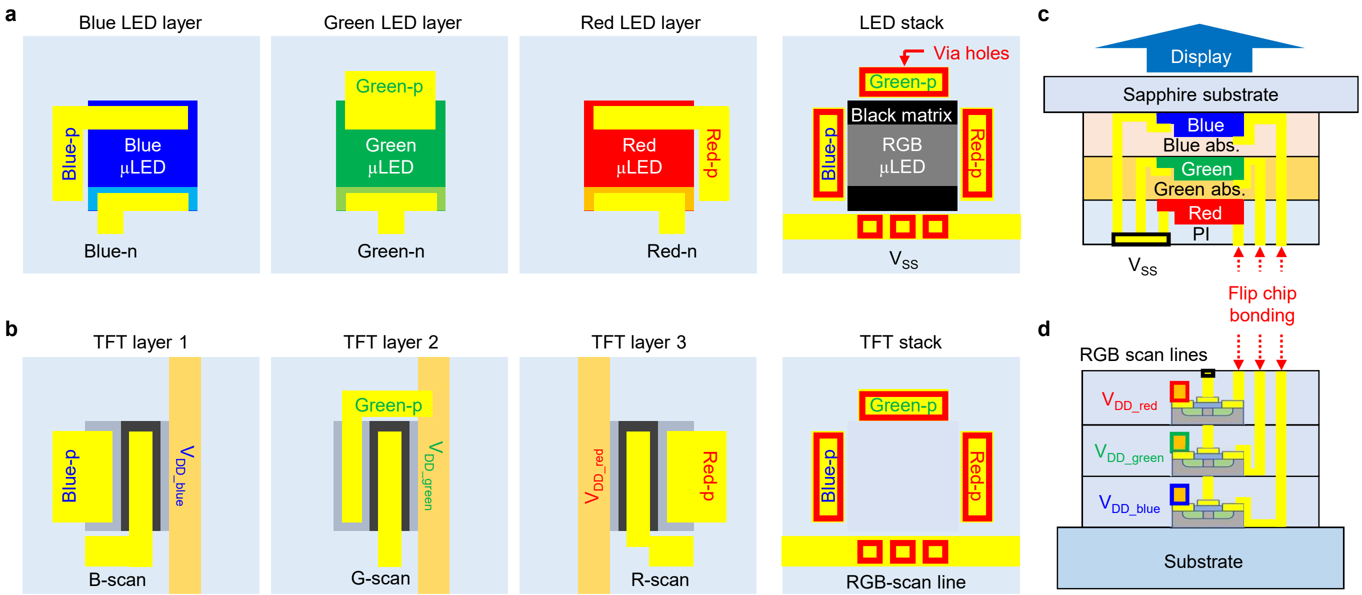

Supplementary Figure 9 | Design plans for full color, vertically stacked active matrix µLED displays. a-d, Schematic layer designs for vertically stacked RGB µLEDs and TFTs as observed from the top (a, b) and from the side (c, d). Ultrathin µLEDs layers are stacked and fabricated on double side polished sapphire substrate, with the blue LED at the bottom and red LED on top, while TFT stacks are formed on a separate substrate. Formation of via holes (red rectangles in a, b) through encapsulating polymer layers, deposition of thick metal film, and planarization of the top surface via CMP yield vertically stacked µLEDs and TFTs for integration via flip chip bonding. Each p-contact of the stacked RGB µLEDs is electrically connected (via flip-chip bonding, for instance) to the source contacts of three vertically stacked Si TFTs, while the n-contacts share a common V_{SS} line. The drain contacts of vertical TFTs form three separate data lines (V_{DD}) for each LED color, while the gate contacts share a common scan line for each RGB pixel. The RGB LEDs may be viewed through the double side polished sapphire substrate.

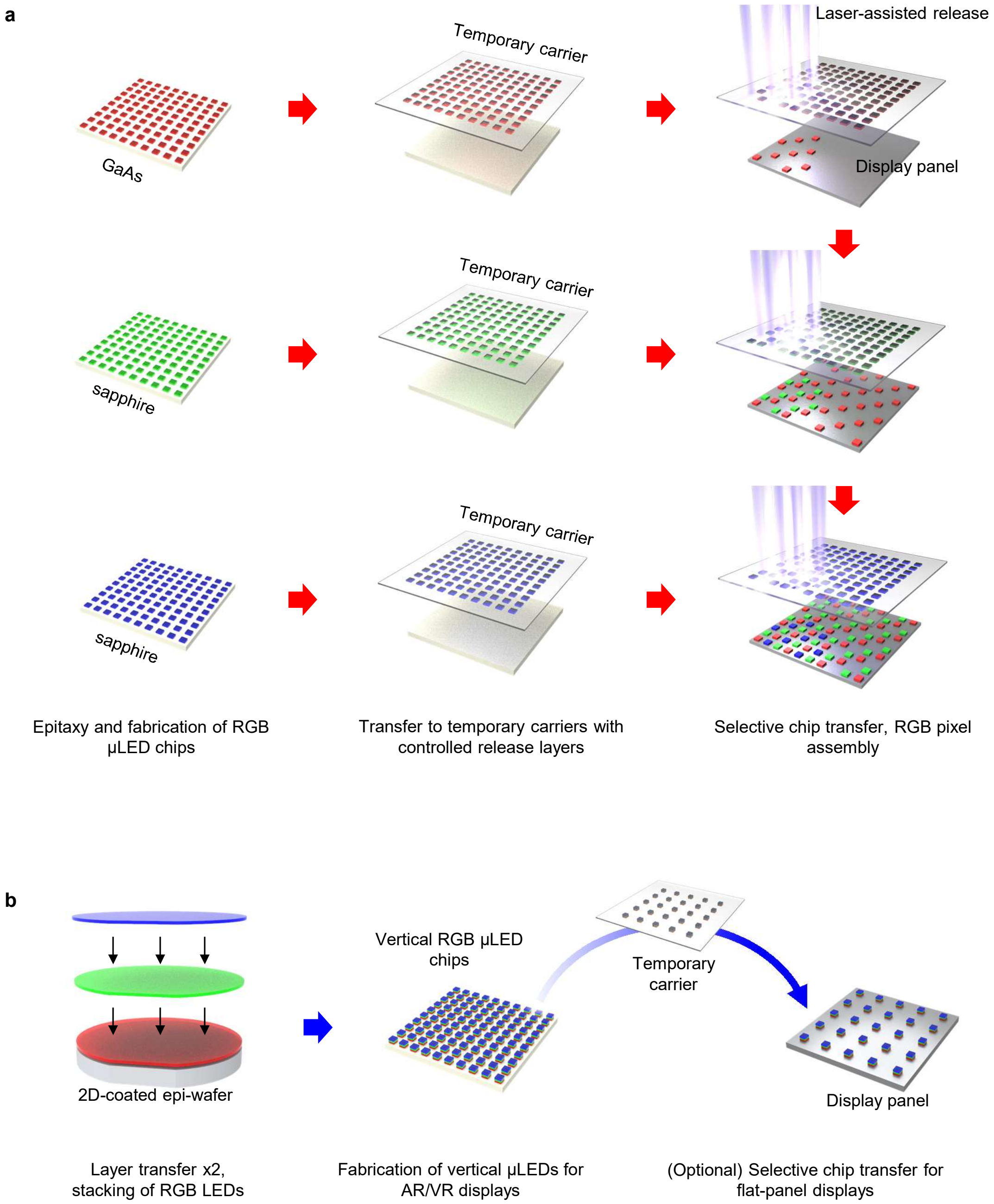

Supplementary Figure 10 | Comparison of conventional pick-and-place process with 2DLT-based chip transfer process. a, Schematic representation of conventional laser-assisted chip transfer process for manufacturing µLED displays, involving multiple transfer steps. **b**, Schematic illustration of 2DLT-based chip transfer process for vertical RGB µLEDs, involving two layer transfers and a single chip transfer.

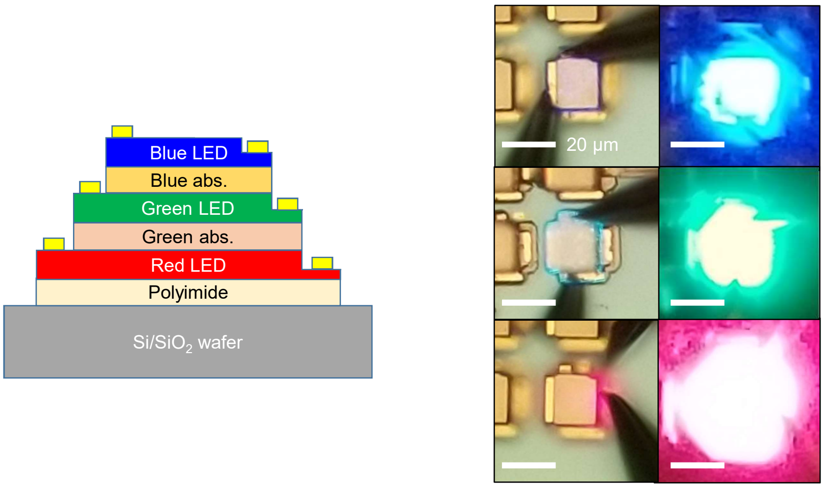

Supplementary Figure 11 | Schematic diagram and optical and EL microscopy images of fully isolated vertical RGB µLED chips.

Supplementary Table 1 | Benchmark of full-color and mono-color µLED displays reported in news articles.

Type	Company, Product (Year)	Subpixel size (µm)	Pitch (µm)	PPI
RGB, vertical	Sundiode, Full-color Microdisplays based on Stacked 3-color Micro-LEDs (2021)	n/a	100	200
RGB, lateral	LG, 163-inch Micro LED TV (2020)	n/a	930	n/a
	PlayNitride, 11.6-inch Automotive Micro LED Display (2021)	n/a	n/a	228
	Sony, Modular Crystal LED Display (2021)	n/a	1260	n/a
	Samsung, 110-inch Micro-LED TV (2021)	75 × 100 (RGB)	630	n/a
Mono color + CC, lateral	AU Optronics (AUO), 12.1-inch Full-color Micro-LED Display Prototype (2018)	< 30	n/a	169
Mono color	Plessey, 2.5-micron Pitch Micro-LED Microdisplay (2019)	n/a	2.5 (blue)	n/a
	Jade Bird Display (JBD), 10000-ppi Micro-LED Microdisplay (2020)	n/a	2.5 (blue) 5.0 (green)	10000 (blue) 5000 (green)

Other Supplementary Materials for this manuscript include the following:

Supplementary Video 1. Exfoliation of blue LED film from hBN-sapphire wafer.

Supplementary Video 2. Electroluminescence of mixed colors for vertical micro-LEDs.